



HAL
open science

Heat transfer inside a blocked region of a rod bundle during a LOCA-simulations and experiments

Juan David Peña Carrillo, Michel Gradeck, Alexandre Labergue, Tony Glantz, Georges Repetto

► **To cite this version:**

Juan David Peña Carrillo, Michel Gradeck, Alexandre Labergue, Tony Glantz, Georges Repetto. Heat transfer inside a blocked region of a rod bundle during a LOCA-simulations and experiments. 9th World Conference on Experimental Heat Transfer, Fluid Mechanics and Thermodynamics (EXHFT-9), Jun 2017, Iguazu, Brazil. hal-03530191

HAL Id: hal-03530191

<https://hal.univ-lorraine.fr/hal-03530191v1>

Submitted on 17 Jan 2022

HAL is a multi-disciplinary open access archive for the deposit and dissemination of scientific research documents, whether they are published or not. The documents may come from teaching and research institutions in France or abroad, or from public or private research centers.

L'archive ouverte pluridisciplinaire **HAL**, est destinée au dépôt et à la diffusion de documents scientifiques de niveau recherche, publiés ou non, émanant des établissements d'enseignement et de recherche français ou étrangers, des laboratoires publics ou privés.

HEAT TRANSFER INSIDE A BLOCKED REGION OF A ROD BUNDLE DURING A LOCA – SIMULATIONS AND EXPERIMENTS

Juan David Peña Carrillo*, Michel Gradeck, Alexandre Labergue
Laboratoire d'Energétique et de Mécanique Théorique et Appliquée, LEMTA
Université de Lorraine, Nancy, France
*penacarr1@univ-lorraine.fr

Tony Glantz, Georges Repetto
Institut de Radioprotection et de Sureté Nucléaire, IRSN
Cadarache, Saint Paul lez Durance, France

Abstract.

This study focuses on the coolability of a partially deformed fuel assembly of a PWR reactor through an accident causing the loss of coolant primary (LOCA). Beyond the dryout point during the reflooding phase, the core is cooled mainly by a vapor/droplets flow. The thermal-hydraulic features of this two-phase flow, as well as the damaged cladding characteristics, are important parameters to estimate the core coolability through the fuel assemblies. In order to analyze experimentally the influences of the cladding deformation on the heat transfer by a vapor/droplet flow, a set-up is developed at the sub-channel scale. Measurements are carried out using optical techniques to characterize the droplet's flow. Along the blocked zone, temperature measurements of the tube surface are performed in order to estimate the total internal heat transfer. One-dimensional mechanistic model, accounting for the heat transfer mechanisms in a post-dryout region, is also developed. This is a necessary step in order to analyze correctly the experimental data and it helps us to better understand heat transfer within the tube.

Keywords: LOCA, Heat transfer, LIF, PDA, drop impact

1. INTRODUCTION

One of the design-related accidents of a PWR reactor is the LOCA (Loss Of Coolant Accident). Such an accident can be caused by a breach on the primary circuit of the reactor resulting in a loss of water inventory, and consequently in a drying of the fuel assemblies. As a result, a considerable increase in temperature would occur within the core of the reactor. Thus, the fuel rod claddings may possibly deform and blocked zones can appear (Figure 1) (Repetto et al. 2015). During the reflooding phase, which aims to cool down and to preserve the integrity of the core reactor, cold water is injected through the assemblies; three zones can be identified depending on the type of flow: (i) a saturated liquid zone, where the first boiling mechanisms are observed; (ii) a post-dryout zone composed of superheated vapor and dispersed droplets. Finally, when all the droplets disappear because of the evaporation, (iii) a monophasic zone of superheated vapor. The coolability of the core during the reflooding by the emergency cooling backup systems (ECCS) is a complex thermal-hydraulic phenomenon which depends on the thermal-hydraulics features of the flow and the damaged cladding characteristics (blockage ratio, blockage length) (Figure 2).

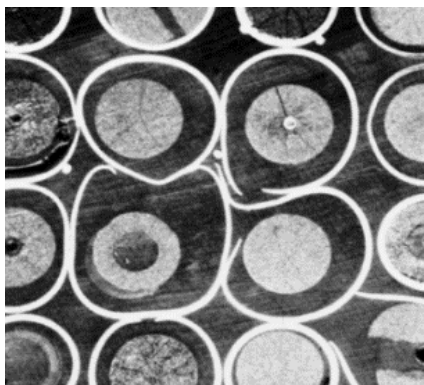


Figure 1. Bundle of deformed fuel rods Phebus LOCA experiments (Repetto et al. 2015)

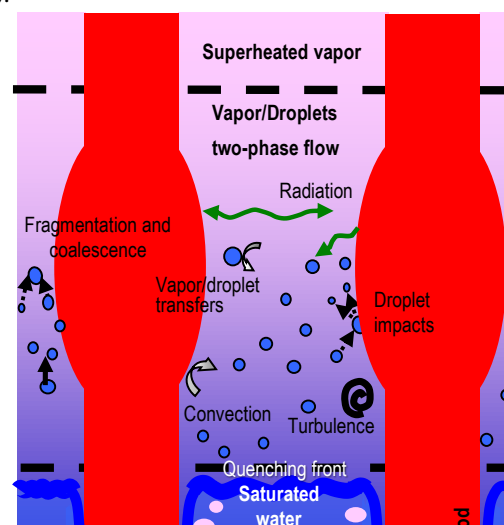


Figure 2. Local phenomena involved in the process

To understand and analyze heat transfer in close LOCA conditions, a new set-up has been built. It will focus on the characterization of two-phase flows with heat and mass transfer in blocked structures at representative sub-channel scale. The use of specific instrumentation such as Laser Induced Fluorescence (LIF), Phase Doppler Anemometry (PDA) and infrared Camera (IR) technics will help to perform accurate balances, particularly those concerning heat and mass transfers.

In order to perform the pre-calculation of the tests foreseen in the set-up and to model the cooling, a one-dimensional mechanistic model will be presented in this paper for two-phase flow taking into account the different mechanisms of heat and mass transfers in the case of a post-dryout regime (Forced convection, radiation and droplet impact in Leidenfrost regime). This model is based on a set of conservation equations (mass, momentum, and energy) which is coupled to transport equations. A set of closure relations will allow estimating the respective part of the different heat transfer mechanisms involved in the cooling.

2. EXPERIMENTAL APPROACH

The proposed approach is expected to understand and quantify experimentally the heat transfer between the dispersed two-phase flow and the heated walls. The experimental test channel is a vertical tube of Inconel-625 (Nickel and chrome alloy with a low degree of oxidation at high temperatures), representative of a blockage zone. In order to reproduce the geometry of the partially blocked zones, a typical venturi configuration was chosen: an internal diameter of the tube upstream and downstream of 11.78 mm, equivalent to the hydraulic diameter of a non-deformed representative sub-channel ($D_h=4P_c/S_{nbal}$). A sub-channel is defined as the fluid domain between four adjacent fuel rods. The blockage ratio is defined as $(1-S_{bal}/S_{nbal})$. The constricted section of the Venturi has an internal diameter equivalent to the hydraulic diameter of a deformed representative sub-channel (Figure 3). The angle of the convergent and divergent part of the venturi is 6° in the present study. Different ratios and lengths of ballooning will be studied (See Table I)

Table I. Geometrical configurations of the constricted section to be tested

	Config. n°1	Config. n°2	Config. n°3	Config. n°4	Config. n°5
Blockage ratio	0%	61%	61%	90%	90%
Equivalent hydraulic diameter	11.78 mm	7.35 mm	7.35 mm	3.72 mm	3.72 mm
Height of the ballooned area	-	100 mm	300 mm	100 mm	300 mm

2.1 Experimental procedure

The partially blocked section of the tube is heated up to 800°C by Joule effect using an electric generator (TDK Lambda Genesys2U series GEN 10-330, 3,3 kW max). When the operating temperature is reached, the injection of the two-phase flow is started. The superheated vapor/droplet flow is injected upstream of the tube in order to cool down the tube. The vapor flow is produced using a vapor generator (AURA MA-6 kW®) able to produce vapor at a maximum temperature of 180°C and a maximum mass flow rate of 8,4 kg/h; At the outlet of the vapor generator, a heater can increase the vapor temperature up to 250°C (AURA S2000 - 2 kW®). The dispersed phase is produced by a piezoelectric injector (FMP Technology®) able to generate calibrated drops at different frequencies. The range of thermal hydraulics parameters available in the present test facility is shown in Table II

Table II. Thermal-hydraulic conditions for the present set-up

Inlet vapor velocity	Up to 15 m/s
Inlet vapor temperature	180°C - 300°C
Inlet droplet velocity	Up to 10 m/s
Inlet droplet temperature	From 25°C to saturation temperature
Droplet diameter	From $50\ \mu\text{m}$ to $250\ \mu\text{m}$
Tube temperature before flow injection	Up to 800°C
Volumetric droplet fraction	0 to $10^{-2}\ \text{m}^3\text{eau}/\text{m}^3$

Pressure, temperature, and volumetric flow will be measured thanks to different sensors; it will allow the estimation of the properties of vapor at the inlet of the tube. Measurements of the droplet characteristics will be carried out upstream and downstream the constricted section of the tube. The properties of dispersed flow (diameter, z-axis velocity, and droplet diameter distribution) will be performed using a Phase Doppler system (PDA). The Phase Doppler system is a 2D commercial classic PDA manufactured by Dantec-Dynamics®. PDA excitation volume is formed by the intersection of two laser beams coming from an argon laser source, ($\lambda = 514.5\text{nm}$). The system includes a classic PDA receiver which

operates in the first refraction mode. The droplet temperature is performed using the Laser Induced Fluorescence (LIF) technique. This technique is based on the measurement of the intensity of fluorescence emitted by a temperature-sensitive fluorescent dye diluted in the water droplets flow. For this case, sulforhodamine-B is used because of its temperature sensibility and for its solubility in water. The fluorescence is induced by the green line of an argon ion laser, the same used for PDA measurement. The temperature of the superheated vapor will be also measured upstream and downstream of the tube via insulated thermocouples. The outer surface temperature of the tube is estimated using an infrared camera (Cedip® Jade III) built with a focal plane array photonics detectors (InSb) working in the spectral range [3 μm –5 μm] ; a narrow-bandwidth [3.97 μm –4.01 μm] spectral filter can be also used to fit with the expected experimental temperature range. The transient cooling of the tube will be thus analyzed by performing coupled measurements of LIF, PDA, and infrared camera (Labergue et al. 2017)

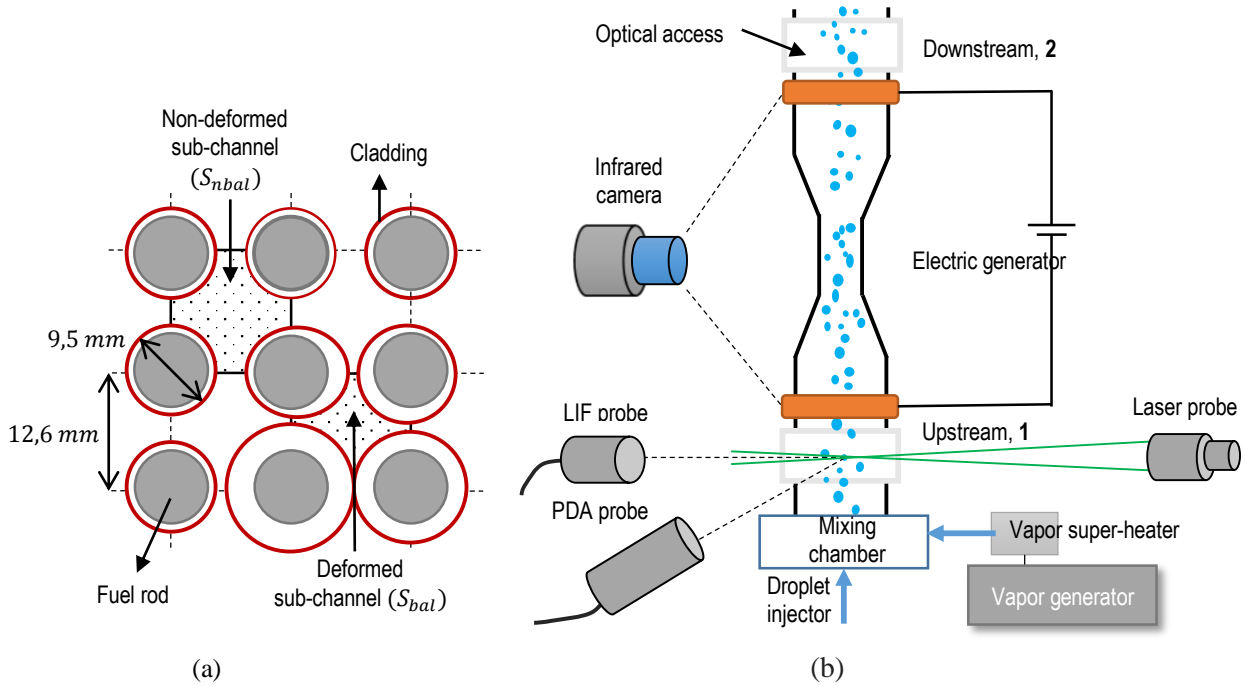


Figure 3. (a) Representation of a partial damaged PWR assembly, (b) Thermal-hydraulic circuit of the experimental set-up

2.2 Energy balance

A simplified expression of the energy balance of the heat fluxes involved in the wall to fluid interactions along the blocked region (I.e between points 1 and 2, Figure 3b), can be written as follows:

$$Q_{wall}(t) = Q_l(t) + Q_v(t) \quad (1)$$

Q_l and Q_v reads :

$$Q_l(t) = (\dot{m}_d - \dot{m}_{ev}(t))C_{pl}(\Delta T_d(t)) + \dot{m}_{ev}(t)C_{pl}(T_{sat} - T_{d,1}(t)) + \dot{m}_{ev}(t)(L_v + C_{pv}[T_{v,2}(t) - T_{sat}]) \quad (2)$$

$$Q_v(t) = \dot{m}_v C_{pv}(\Delta T_v(t)) \quad (3)$$

The two first expressions in the RHS of equation 2 correspond to the sensible heat gained by the liquid, and the last one to the phase change and sensible heat gained by the evaporated mass (\dot{m}_{ev}). ΔT_d is the increase in the droplet temperature, and $T_{d,1}$ is the droplet temperature upstream the tube, both measured by LIF technique. ΔT_v is the increase in the vapor temperature, measured using thermocouples. Q_{wall} , can be estimated using the following relation:

$$Q_{wall}(t) = Q_{Joule} - Q_{ext} - \rho_{tube} V_{tube} C_{p,tube} \frac{dT_w(t)}{dt} \quad (4)$$

Where Q_{Joule} , is the internal heat generation (by Joule effect). Q_{ext} represents the external losses associated with the natural convection, the heat conduction within the sample holder, and the radiative transfer to the surroundings. It can be

estimated experimentally during the cooling of the tube without any flow ($Q_{wall}=0$); dT_w/dt is the variation in mean surface temperature over time, measured by infrared camera.

Introducing the Jacob number $Ja(t) = C_{pv}(\tilde{T}_{v,2}(t) - T_{sat})/L_v$, and arranging equations 1, 2, and 3, \dot{m}_{ev} is obtained:

$$\dot{m}_{ev}(t) = \frac{Q_{wall}(t) - \dot{m}_d C_{pl}(\Delta T_d(t)) - \dot{m}_v C_{pv}(\Delta T_v(t))}{C_{pl}(T_{sat} - T_{d,2}(t)) + L_v(1 + Ja(t))} \quad (5)$$

In this way, it is possible to determine the amount of evaporated mass and thus calculate the different heat transfers contributions involved in the cooling of the wall by the two-phase flow (I.e Q_l and Q_v). In addition, thanks to PDA measurements, it will be possible to follow the dynamic characteristics of the droplet flow upstream and downstream the blocked section (velocity, diameter, and droplet distribution)

3. MODEL APPROACH

In order to complement and understand the experimental data, a mechanistic model has been developed. The present model, composed of conservation of mass, conservation of momentum, conservation of energy, as well as a system of transport equations, will allow estimating the respective part of the different heat transfer mechanisms involved across the channel. In order to simplify the calculation, the following assumptions are made:

- One-dimensional flow
- Droplets are at saturation temperature
- Liquid droplets have a spherical shape
- No droplet break-up and coalescence
- No vapor flow separation in the expansion area
- No turbulent forces are taken into account

3.1 Heat transfers mechanisms in post-dryout region

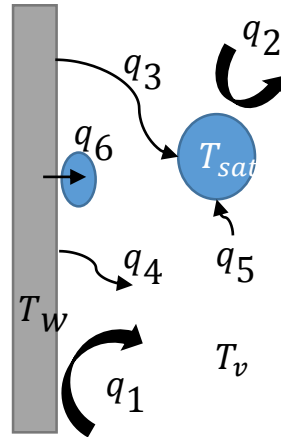


Figure 4. Heat transfers mechanisms in post-dryout region for a two-phase flow

As shown in Figure 4, six heat transfers mechanisms in the post-dryout region are of major importance in the analyses of vapor/droplet flows. Several prediction methods of these heat transfers mechanism are proposed in the literature (Guo & Mishima 2002; Wang et al. 2015; Li & Anglart 2016). The correlations used in the present model are presented below:

Wall to vapor forced convection (q_1): The heat flux extracted at the wall by the vapor can be expressed as follows

$$q_1 = h_1 (T_w - T_v) \quad (6)$$

Gnielinski (Meholic 2011) proposes a model predicting the heat transfer coefficient h_1 :

$$h_1 = \left(\frac{\lambda_v}{D_h} \right) \frac{(f_f/8)(Re - 1000)Pr}{1 + 12,7(f_f/8)^{0,5} (Pr^{2/3} - 1)} \left(\frac{T_v}{T_w} \right)^{0,45} \quad (7)$$

Where Re is based on the tube diameter and on the vapor velocity. We consider a smooth pipe to estimate f_f

Vapor to droplet interfacial convection (q_2): The interfacial vapor to droplet heat flux can be expressed as follows:

$$q_2 = h_2 (T_v - T_{sat}) \quad (8)$$

Experimentally, it has been shown that the evaporation decreases the heat transfer between vapor and drops (Lee et al. 1984) (Yuen & Chen 1978). To take this into account, the following correlation is used (Ban & Kim 2000):

$$h_2 = \left(\frac{\lambda_v}{d} \right) \frac{2 + 0,74Re_g^{0,5} Pr^{1/3}}{1 + B_T} \quad (9)$$

Where Re_g is based on the droplet diameter and on the relative velocity between the vapor and droplet, and B_T is the mass transfer number defined as:

$$B_T = \frac{C_{pv}(T_v - T_{sat})}{L_v} \quad (10)$$

Wall to fluid and fluid to fluid radiation ($q_3, q_4, \text{ and } q_5$): The heat flux exchanged between the wall and the two-phase flow is a coupled phenomenon that takes into account the optical, geometric and thermal properties of each medium. In order to estimate these contributions, and considering a gray and diffuse mixture of vapor-droplets in the optically thin regime, the Sun's model (Sun et al. 1976) is used in the present work to characterize the thermal radiation:

$$q_3 = \omega_{w-d} \sigma_b (T_w^4 - T_{sat}^4) \quad (11)$$

$$q_4 = \omega_{w-v} \sigma_b (T_w^4 - T_v^4) \quad (12)$$

$$q_5 = \omega_{v-d} \sigma_b (T_v^4 - T_{sat}^4) \quad (13)$$

Where ω is the gray-body factor, and depends on the emissivity of the medium and the wall and can be estimated using the following equations:

$$\varepsilon_v = 1 - e^{-a_v D_h} \quad (14)$$

$$\varepsilon_d = 1 - e^{-a_d D_h} \quad (15)$$

In our case, the wall emissivity is about 0.6. The vapor emissivity, taking into account the assumption of an optically thin medium, can be estimated directly using one of the correlations given in the literature (Siegel & Howell 1992). The droplet absorption coefficient (a_d) is given using the following equation (Sun et al. 1976)

$$a_d = \frac{1,12\alpha_d}{d} \quad (16)$$

Wall to droplet direct contact heat transfer (q_6): Since the wall temperature is above the Leidenfrost temperature, a vapor layer forms between the droplet and the wall during the impingement. Also, for low Weber numbers, characteristic of LOCA condition (below a critical value of the order of 30), a pure rebound phenomenon without droplet break-up can be observed. Using these assumptions, (Guo & Mishima 2002) developed a model taking into account the heat transfer by conduction between the wall and the droplet through the vapor layer:

$$q_6 = (T_w - T_{sat}) \left(\frac{18\lambda_v^3 t_r^3 \rho_v L_v \dot{m}_{dep}^5}{d^5 \rho_d^4 \mu_v \alpha_d (T_w - T_{sat})} \right)^{1/4} \quad (17)$$

Where \dot{m}_{dep} is the droplet deposition rate of droplets migrating towards the wall. The deposition model of Hewitt (Li & Anglart 2016) is used in this work:

$$\dot{m}_{dep} = \begin{cases} \frac{0.18\alpha_d \rho_d}{\sqrt{\frac{\rho_v D_h}{\gamma}}} \text{ if } \frac{\alpha_d \rho_d}{\rho_v} < 0.3 \\ \frac{0.083(\alpha_d \rho_d)^{0.35} \rho_v^{0.65}}{\sqrt{\frac{\rho_v D_h}{\gamma}}} \text{ if } \frac{\alpha_d \rho_d}{\rho_v} > 0.3 \end{cases} \quad (18)$$

With t_r the droplet residence time suggested by Biance (Biance et al. 2006)

$$t_r = 2.65 \sqrt{\frac{\rho_d d^3}{8\gamma}} \quad (19)$$

3.2 Momentum balance of droplets

Because of the high droplet density compared to the vapor phase, the droplets are accelerated mainly by the effect of the drag force (added mass force neglected). Thus, the following correlation allows to calculate the z-axis evolution of the droplet velocity:

$$u_d \rho_d \frac{du_d}{dz} = -\frac{3}{4d(1+B_T)} \theta C_d \rho_v (u_d - u_v) |u_d - u_v| + (\rho_v - \rho_g)g \quad (20)$$

Where C_d is the drag coefficient of a droplet. The following correlation allows to estimate it (Morsi & Alexander 1972):

$$C_d = \frac{A1}{Re^2} + \frac{A2}{Re} + A3 \quad (21)$$

$A1$, $A2$, and $A3$ are constants which depend on Reynolds number based on the droplet diameter. As in the case of the calculation of h_2 , the drag coefficient is reduced by the evaporation effect $1/(1+B_T)$. The coefficient θ , correct the drag coefficient of an isolated droplet taking into account the influence of the dispersed phase concentration (Oesterlé 2006):

$$\theta = \frac{1}{1 - 6.55\alpha_d} \quad (22)$$

3.3 Energy balance of vapor

In order to estimate the increase in vapor temperature, energy balance is performed taking into account the heat transfers mechanisms described previously:

$$\Delta T_v = \frac{Q_1 + Q_4 - (Q_2 + Q_5)}{C_{pv}(\dot{m}_v + \dot{m}_{ev})} - T_v \left(1 - \frac{\dot{m}_v}{\dot{m}_v + \dot{m}_{ev}} \right) \quad (23)$$

Where \dot{m}_{ev} is the evaporated droplet mass flux (When the droplets reach the saturation temperature):

$$\dot{m}_{ev} = (Q_2 + Q_3 + Q_5 + Q_6)/L_v \quad (24)$$

3.4 Transport equations

In order to estimate the axial evolution of important volumetric parameters (i.e. volumetric interfacial area a_{int} , volumetric liquid fraction α_d) the transport equation for η th moment density is defined as (Morel et al. 2010):

$$\frac{d(S_\eta u_{d,\eta})}{dz} = \eta S_{\eta-1} G_{\eta-1} + \psi_\eta \quad (25)$$

The first term on the right-hand side represent the change in volume of droplets (Due to evaporation for our case) and the second term, ψ , the source term due to droplet break-up and coalescence, neglected in this study because of the low volumetric liquid fraction and Weber number. S_η , $u_{d,\eta}$, and G_η are defined as (Morel et al. 2010):

$$\begin{aligned} S_\eta &= n \int_0^\infty P(d) d^\eta dd \\ u_{d,\eta} &= \int_0^\infty P(d) u_d(d) d^\eta dd \Big/ \int_0^\infty P(d) d^\eta dd \\ G_\eta &= \int_0^\infty P(d) \dot{G}_d(d) d^\eta dd \Big/ \int_0^\infty P(d) d^\eta dd \end{aligned} \quad (26)$$

Where $P(d)$ is the droplet diameter distribution (which will be discussed in the next section), n denotes the droplet concentration (Number of droplets per unit volume), u_d is the droplet velocity and \dot{G}_d is the particle size change due to evaporation (dd/dt , (m/s)); in order to estimate G_η , the following correlation is used, $\dot{G}_d(d) = b_1 d^{b_2}$, Where b_1 and b_2 are constants which depend on the local thermal-hydraulic features. Making successively $\eta=0,1,2,3$ in equation (21), four transport equations allow to solve S_0, S_1, S_2 , and S_3 , and thus n , a_i and α_d can be determined ($n=S_0; a_{int}=\pi S_2; \alpha_d=\pi S_3/6$)

3.5 Droplet diameter distribution

A log-normal droplet distribution is adopted in the present work, and defined as (Kamp et al. 2001):

$$P(d) = \frac{1}{\sqrt{2\pi}\sigma d} e^{-\frac{\left(\ln\left(\frac{d}{d_{oo}}\right)\right)^2}{2\sigma^2}} \quad (27)$$

Where σ , is the standard deviation of the natural logarithm and d_{oo} the mean characteristic diameter. Thus, it is possible to define the PDF at any point of the tube by knowing only these two parameters which depend on the first and second-moment densities, as well as α_d , calculated using the equation (21):

$$\begin{aligned} \sigma &= \sqrt{\ln\left(\frac{6\alpha_d S_1}{\pi S_2^2}\right)} \\ d_{oo} &= \frac{6\alpha_d}{\pi S_2} e^{-\frac{5}{2}\sigma^2} \end{aligned} \quad (28)$$

Discretization of droplet distribution: In order to consider the droplet distribution in heat transfer as well as axial dynamic calculations, the distribution is divided into bins of equal volume (Meholic et al. 2015). The equations presented in subsections 3.1 and 3.2 are solved for each bin using the equivalent bin Sauter diameter, defined as:

$$d_{32i} = \int_{d_{low}}^{d_{up}} P(d) d^3 dd \Big/ \int_{d_{low}}^{d_{up}} P(d) d^2 dd \quad (29)$$

4. MODEL APPLICATION

The equations presented previously are solved numerically to obtain the distributions of droplet size, volumetric void fraction and vapor temperature along the channel and thus estimate each one of the heat transfers inside the tube.

4.1 Geometry and flow features

In this paper, a vertical tube of 0.5 m long will be considered (Figure 6). Configurations 1, 3, and 5 will be analyzed from Table I (I.e. internal diameter of 11.78 mm, 7.35 mm, and 3.72 mm for a length of 0.3 m). An imposed temperature of 800°C is used as wall boundary condition. At the inlet of the domain, the next conditions are imposed:

Table III. Thermal-hydraulic imposed conditions at the bottom inlet of the domain

Droplet velocity (m/s)	Vapor velocity (m/s)	Droplet temperature (°C)	Vapor temperature (°C)	Volumetric droplet fraction (-)	P (bar _a)	σ	d_{oo} (μm)	N_{bins}
10	12	T_{sat}	250	0.001	2	0.10	100	10

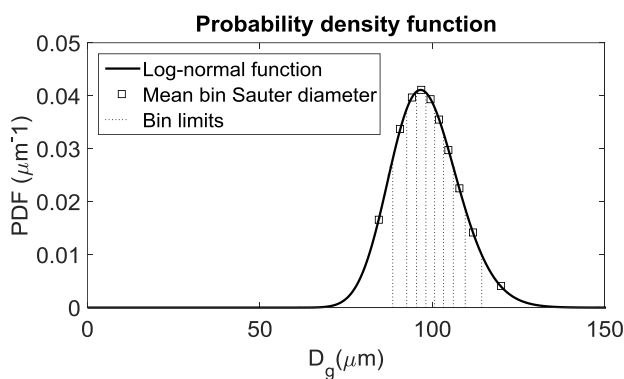


Figure 5. Droplet distribution imposed at the inlet domain ($\sigma=0.10$ and $d_{oo}=100 \mu\text{m}$. 10 bins)

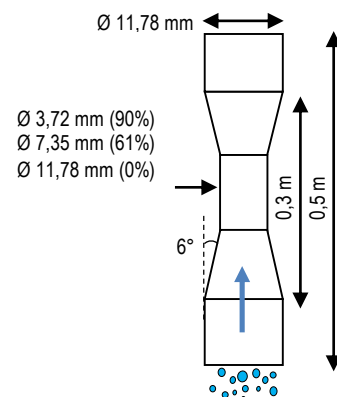


Figure 6. Geometry of calculation domain

4.2 Two-phase flow characteristics

Figure 7a shows the vapor temperature axial evolution for three different blockage ratios. Vapor temperature is more important when the blockage ratio increases. Upstream the contracted zone, the vapor undergoes a small reduction in temperature because of a large part of its energy is transferred to the dispersed droplet phase, due to a local increase of the volumetric droplet fraction in the convergent part of the venturi tube. In general, for the three configurations analyzed here, the vapor temperature increases axially because of an increasing in vapor mass flow by the evaporation of a part of the droplets flow, and also due to the thermo-dependence effect of the vapor causing a vapor acceleration and improving mainly the wall to vapor heat transfer. In the case of the 61% and 90% blockage, the increase in temperature is mainly due to the reduction of the cross-sectional flow area and, as a result, high velocities are expected in the contracted part improving the total wall to vapor heat transfer.

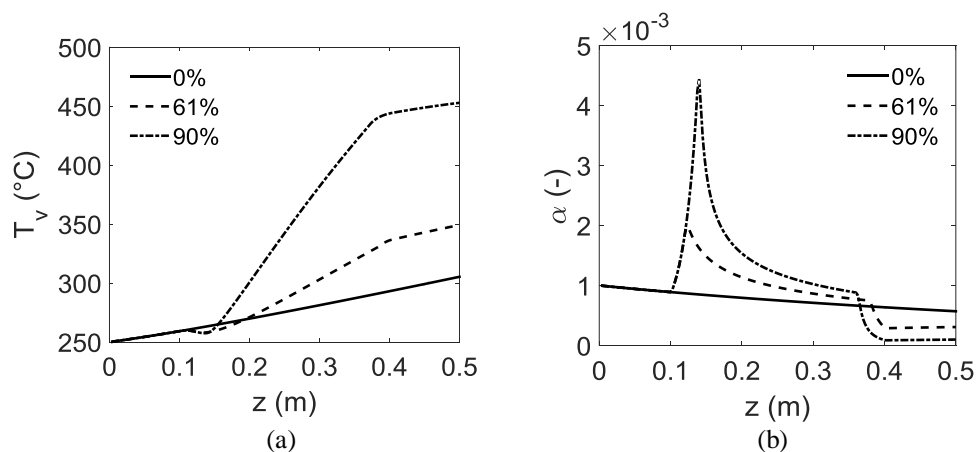


Figure 7. (a) Longitudinal evolution of vapor temperature, (b) longitudinal evolution of volumetric droplet fraction

Figure 7b shows the volumetric droplet fraction α_d axial evolution. In the case of a non-blocked tube, a reduction of the droplet fraction is produced by the loss in volume of the dispersed flow due to the evaporation. For the two blockage configurations analyzed, the droplet fraction increases in the contracted zone and decreases downstream.

The axial evolution of d_{00} (Log-normal mean characteristic diameter) is shown in Figure 8a. For the three cases analyzed here, d_{00} decreases because of the droplet evaporation. The diameter decreases more in the case of non-blockage because the droplets are less accelerated compared to blocked configurations, thus the dispersed flow takes more time to cross the domain and the evaporated mass flux is more important. As shown in Figure 8b, droplet evaporation causes an increase in the vapor mass flow of 21%, 19%, and 17% for a blockage ratio of 0%, 61%, and 90% respectively.

Figure 8c shows the droplet diameter distribution upstream and downstream for a non-blocked tube (0%). As would be expected, the downstream PDF moves towards the left compared to the upstream PDF due to the evaporation of the drops, an effect that reduces its diameter. The mean characteristic diameter d_{00} is reduced from 100 μm to 92 μm , while the standard deviation σ changes only from 0.1 to 0.103. A similar displacement of the PDF toward the left was obtained for the configurations of 61% and 90% blockage.

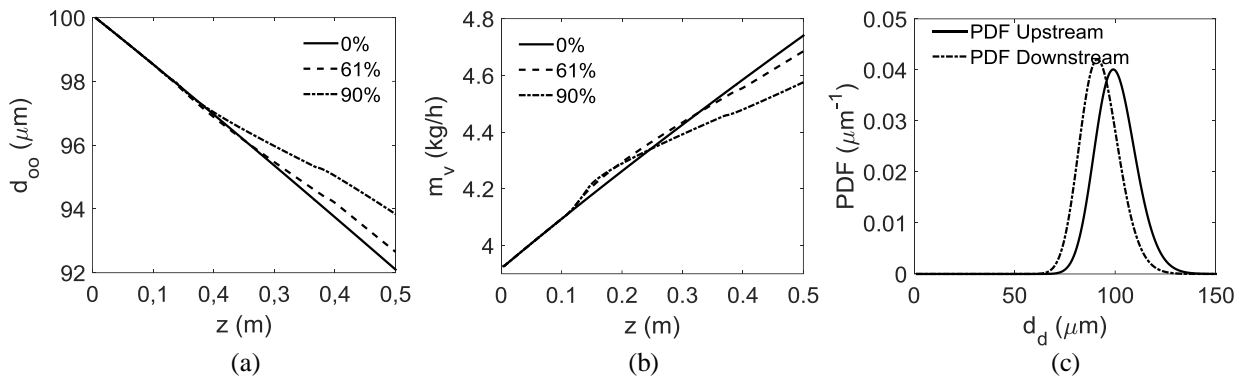


Figure 8. (a) Longitudinal evolution of characteristic log-normal diameter d_{00} ; (b) longitudinal evolution of vapor flux mass (c) PDF of the droplet diameter upstream and downstream the tube, non-blocked configuration

Heat transfers

In order to analyze the different heat transfer mechanisms, wall to fluid heat transfers for 0% and 61% blockage are shown in Figure 9. The most important heat transfer contribution along the tube is wall to vapor forced convection (q_1). For the non-blocked case, q_1 increases due to the evaporated flux mass and also by thermo-dependency of superheated vapor which causes an increasing in vapor velocity; For the case of 61% blockage ratio, the contribution of q_1 is much more highlighted due to the significant increase in the vapor velocity because of the vapor acceleration in the intermediate part of the tube. Wall to droplet radiation q_3 plays an important role and its axial evolution is related to the volumetric liquid fraction. Wall to vapor radiation q_4 has also an important contribution, it remains almost constant for a non-blocked tube and is reduced a little in the blocked region. For our study case, wall to droplet direct contact heat transfer q_6 is the smallest wall to fluid contribution. As well as q_3 contribution, q_6 is highly related to the volumetric droplet fraction; Even if this contribution could be neglected, their consideration is important in situations where α_d is higher. For the purpose of comparing the different heat transfer mechanisms, the spatial-averaged heat transfer is defined as:

$$\tilde{q}_i = \frac{1}{L} \int_0^L q_i(z) dz \quad (30)$$

Table IV shows the spatial-averaged heat transfers of each heat transfer contribution. For all the configuration tested, wall to vapor convective heat transfer q_1 is the most important contribution. This contribution increase as the blockage ratio is more critical representing approximately 68%, 80% and 92% of the total heat flux removed from the wall for configuration 1, 3, and 5 respectively. In fact, the vapor acceleration increases the Reynolds number resulting in an enhancement of the convective heat transfer coefficient h_1 . Wall to fluid radiation (i.e q_3 and q_4), decreases as the blockage ratio is more critical. Their contributions represent 30%, 18% and 7% the total heat flux for configurations 1, 3, and 5 respectively. Wall to droplet direct contact heat transfer q_6 increases a little bit as a function of blockage ratio. Their contribution represents 1.5%, 1.2% and 0.8%. Vapor to droplet heat transfer (q_2) which participates mainly in the evaporation of droplets phenomena, is more important as a function of the blockage ratio because the relative velocity between the two phases is more important as well as the vapor temperature. For all the cases, vapor to droplets radiation (q_5) is very small in quantity.

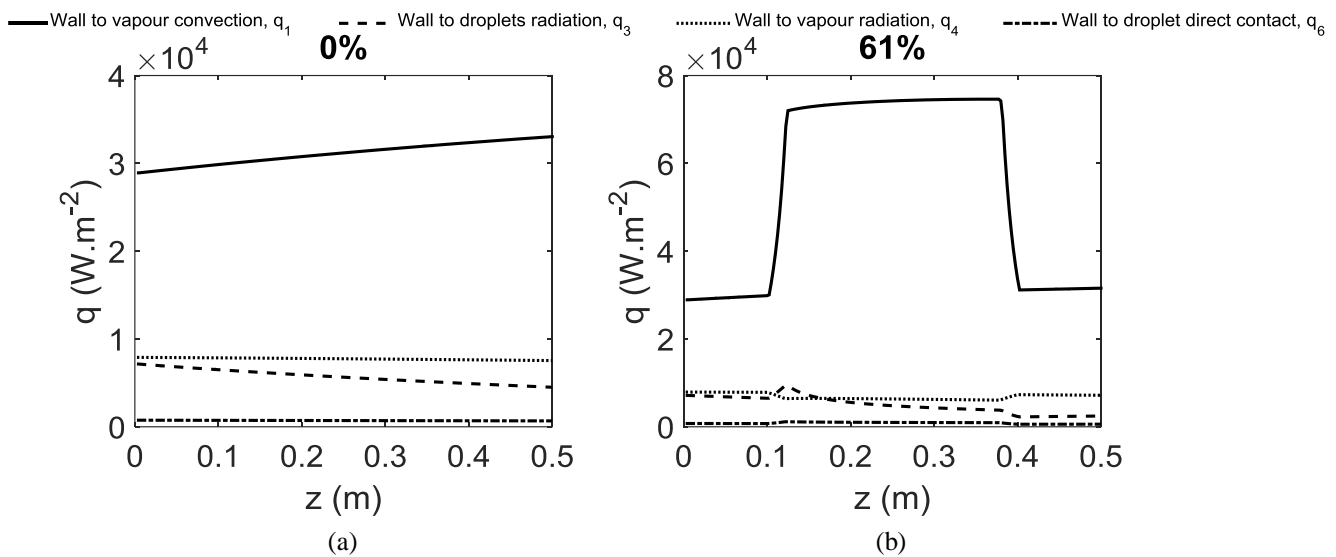


Figure 9. Longitudinal evolution of wall to fluid heat transfers. (a) 0% blockage (b) 61% blockage

Table IV. Spatial-averaged wall to fluid heat transfer and vapor to droplet heat transfer (Equivalent heat transfer per wall unit area)

	Wall to fluid heat flux transfer (kW.m ⁻²)				Vapor to droplet heat flux transfer (kW.m ⁻²)		Total wall to fluid heat transfer (W)
	q ₁	q ₃	q ₄	q ₆	q ₂	q ₅	Q ₁₊ Q ₃₊ Q ₄₊ Q ₆
Configuration 1 (0%)	31.12	5.78	7.74	0.71	24.65	0,025	840
Configuration 3 (61%)	54.26	4.98	6.87	0.853	33.01	0,017	980
Configuration 5 (90%)	131.84	3.98	5.65	1.06	46.05	0.012	1690

5. CONCLUSIONS

To study LOCA conditions closely, a new set-up is built focused on the characterization of two-phase flows with heat transfer through representative deformed sub-channels using specific instrumentation such as Laser Induced Fluorescence, Phase Doppler Anemometry and infrared thermography techniques: A given vapor/droplet flow is injected into the heated tube; upstream and downstream the droplet dispersed flow will be characterized using a PDA device (velocity, diameter, and PDF). Infrared thermography allows estimating the total wall to fluid heat transfer. Thanks to the Laser Induced Fluorescence device is possible to measure the temperature of the droplets and therefore estimate the sensible heat gained by the liquid. Using the measurement data, it will be possible to evaluate the coolability inside a blocked section.

In parallel, a one-dimensional mechanistic model taking into account of the heat transfers mechanism in a post-dryout region is presented in this paper. This model allows estimating the respective impact of the different heat transfer mechanisms involved in the cooling of a heated tube by the two-phase non-equilibrium thermal flow. Three geometrical configurations of the partially blocked section have been analyzed in order to compare the axial distribution of each one of heat transfers mechanism: For all the cases, wall to vapor convective heat transfer is the most important contribution. Wall to fluid radiation contributions also has an important role. Even if wall to droplet direct contact heat transfer could be neglected, their consideration is important in situations where ad is higher.

The present model is expected to be used in order to compare the results that will be obtained experimentally and thus better understand the phenomenon of cooling of a partially deformed section by a vapor/droplet flow. It is also expected to use these results in a wall heat transfer module with the aim of analyzing and predicting the surface temperature over time during the reflooding phase by a vapor/droplet flow.

ACKNOWLEDGMENTS

This work is completed within the framework of RSNR Project from a French State aid managed by the National Agency for Research under the program of Investments for the Future carrying the reference n° ANR-11-RSNR-0017. Particular acknowledgments are also given to EDF for its financial support.

Nomenclature

u	Velocity ($\text{m}\cdot\text{s}^{-1}$)
a_{int}	Volumetric interfacial area (m^{-1})
L_v	Vaporization latent heat ($\text{kJ}\cdot\text{kg}^{-1}$)
\dot{G}	Particle size change ($\text{m}\cdot\text{s}^{-1}$)
\tilde{h}	Enthalpy ($\text{J}\cdot\text{kg}^{-1}\text{K}^{-1}$)
Q	Heat transfer rate (W)
q	Heat transfer flux ($\text{W}\cdot\text{m}^{-2}$)
g	Gravitational constant ($\text{m}\cdot\text{s}^{-2}$)
C_p	Specific heat ($\text{J}\cdot\text{kg}^{-1}\text{K}^{-1}$)
n	Volumetric droplet concentration (m^{-3})
h	Heat transfer coefficient ($\text{W}\cdot\text{m}^{-2}\text{K}^{-1}$)
a	Absorption coefficient
T	Temperature (K)
S	Cross sectional flow area (m^2)
Pr	Prandtl number (-)
Nu	Nusselt number (-)
Re	Reynolds number (-)
α_d	Volumetric liquid fraction (-)
C_d	Drag coefficient (-)
B_T	Mass transfer number (-)
f_f	Friction factor (-)
t_r	Resident droplet time (s)
\dot{m}	Vapor mass flux ($\text{kg}\cdot\text{s}^{-1}$)
d_{oo}	Characteristic diameter (m)

d	Droplet diameter (m)
D_h	Hydraulic diameter (m)
z	Axial position (m)
L	Vertical tube length (m)

Greek symbols

ρ	Density ($\text{kg}\cdot\text{m}^{-3}$)
μ	Dynamic viscosity (Pa.s)
λ	Thermal conductivity ($\text{W}\cdot\text{m}^{-1}\text{K}^{-1}$)
ε	Emissivity (-)
σ_b	Stephan-Boltzmann constant ($\text{W}\cdot\text{K}^{-4}$)
σ	Standard log-normal deviation (-)
ω	Gray body factor (-)
γ	Surface tension ($\text{N}\cdot\text{m}^{-1}$)

Subscripts

<i>bal</i>	Ballooned
<i>d</i>	Droplet
<i>dep</i>	Deposition
<i>ev</i>	Evaporated
<i>nbal</i>	Non-ballooned
<i>sat</i>	Saturation
<i>v</i>	Vapor
<i>w</i>	Wall
<i>low</i>	Lower bin limit
<i>up</i>	Upper bin limit

REFERENCES

- Ban, C.H. & Kim, Y., 2000. Evaporation of a water droplet in high Temperature steam. *Journal of the Korean Nuclear Society*, 32(5), pp.521–529.
- Biance, A.-L. et al., 2006. On the elasticity of an inertial liquid shock. *Journal of Fluid Mechanics*, 554(1), p.47.
- Guo, Y. & Mishima, K., 2002. A non-equilibrium mechanistic heat transfer model for post-dryout dispersed flow regime. *Experimental Thermal and Fluid Science*, 26(6–7), pp.861–869.
- Kamp, A.M. et al., 2001. *Bubble coalescence in turbulent flows: A mechanistic model for turbulence-induced coalescence applied to microgravity bubbly pipe flow*,
- Labergue, A. et al., 2017. Combined three-color LIF-PDA measurements and infrared thermography applied to the study of the spray impingement on a heated surface above the Leidenfrost regime. *International Journal of Heat and Mass Transfer*, 104, pp.1008–1021.
- Lee, R., Reyes, J.N. & Almenas, K., 1984. Size and number density change of droplet populations above a quench front during reflood. *International Journal of Heat and Mass Transfer*, 27(4), pp.573–585.
- Li, H. & Anglart, H., 2016. Prediction of dryout and post-dryout heat transfer using a two-phase CFD model. *International Journal of Heat and Mass Transfer*, 99, pp.839–850.
- Meholic, M.J., 2011. *The development of a non-equilibrium dispersed flow film boiling heat transfer modeling package*. Pennsylvania State University.
- Meholic, M.J., Aumiller, D.L. & Cheung, F.B., 2015. A comprehensive, mechanistic heat transfer modeling package for dispersed flow film boiling - Part 1 - Development. *Nuclear Engineering and Design*, 291, pp.302–311.
- Morel, C. et al., 2010. Comparison of several models for multi-size bubbly flows on an adiabatic experiment. *International Journal of Multiphase Flow*, 36(1), pp.25–39.
- Morsi, S.A. & Alexander, A.J., 1972. An investigation of particle trajectories in two-phase flow systems. *Journal of Fluid Mechanics*, 55(2), p.193–208.
- Oesterlé, B., 2006. *Écoulements multiphasiques : des fondements aux méthodes d'ingénierie*, Lavoisier.
- Repetto, G. et al., 2015. Core Coolability in Loss of Coolant Accident : the Coal Experiments. , pp.24–37.
- Siegel, R. & Howell, J.R., 1992. *Thermal Radiation Heat Transfer*, 3rd edition.
- Sun, K.H., Gonzales-Santalo, J.M. & Tien, C.L., 1976. Calculation of Combined Radiation and Convection Heat Transfer in Rod Bundles Under Emergency Cooling Conditions. *Journal of Heat Transfer*, 98(3), pp.414–420.
- Wang, Y.J., Pan, C. & Energy, C., 2015. Development of a post-dryout heat transfer model. , pp.6890–6903.
- Yuen, M.C. & Chen, L.W., 1978. Heat-transfer measurements of evaporating liquid droplets. *Int.J. of Heat and Mass Transfer*, 21(5), pp.537–542.